

## **CALCULATION OF SHAPE DERIVATIVES WITH PERIODIC FAST MULTIPOLE METHOD WITH APPLICATION TO SHAPE OPTIMIZATION OF METAMATERIALS**

**W. Wang and N. Nishimura\***

Department of Applied Analysis and Complex Dynamical Systems,  
Graduate School of Informatics, Kyoto University, Yoshida Honmachi,  
Sakyo-ku, Kyoto 606-8501, Japan

**Abstract**—This paper discusses computation of shape derivatives of electromagnetic fields produced by complex 2-periodic structures. A dual set of forward and adjoint problems for Maxwell's equations are solved with the method of moments (MoM) to calculate the full gradient of the object function by the adjoint variable method (AVM). The periodic fast multipole method (pFMM) is used to accelerate the solution of integral equations for electromagnetic scattering problems with periodic boundary conditions (PBC). This technique is applied to shape optimization problems for negative-index metamaterials (NIM) with a double-fishnet structure. Numerical results demonstrate that the figure of merit (FOM) of metamaterials can reach a maximum value when the shape parameters are optimized iteratively by a gradient-based optimization method.

### **1. INTRODUCTION**

Metamaterials are a class of composite materials with sub-wavelength structures. It is said that one can control the material properties of metamaterials relatively freely by designing the structure appropriately. Optical negative-index metamaterials (NIM) are particularly interesting, which have negative effective refractive index in the optical range. One may possibly achieve a perfect focusing of light beams with optical NIM (perfect lens) as discussed by Pendry [1]. Early experimental investigations on optical NIMs are found in Zhang et al. [2] who suggested the double-fishnet (DF) grating structure and

---

*Received 31 January 2012, Accepted 2 April 2012, Scheduled 10 April 2012*

\* Corresponding author: Naoshi Nishimura (nchml@i.kyoto-u.ac.jp).

in [3] by Dolling et al. who fabricated a DF structure and tested it at 780 nm wavelength. The reader is referred to Valentine et al. [4] for subsequent developments related to negative index fishnet metamaterials.

It is known, however, that such metamaterials are always with losses whose reduction is very important in the design of metamaterials [5]. Since the imaginary part of the effective refractive index  $n$  indicates the loss, it is required to make the figure of merit (FOM) defined by  $-\text{Re}(n)/\text{Im}(n)$  as large as possible. We are thus lead to an optimization problem which can be described as

$$\max_{\boldsymbol{\tau}} \text{FOM} = -\text{Re}(n(r, t))/\text{Im}(n(r, t)), \quad (1)$$

where  $r = r(\boldsymbol{\tau})$  is the reflection coefficient,  $t = t(\boldsymbol{\tau})$  the transmission coefficient, and  $n$  an effective refractive index retrieved from  $r$  and  $t$  [6], respectively. Also,  $\boldsymbol{\tau} = (\tau_1, \dots, \tau_p)$  is a vector of  $p$  shape design parameters, such as thickness of each layer and line width of the DF grating structure, etc..

Related investigations are found in literature (e.g., [7–9]), which utilize so called stochastic optimization techniques such as genetic algorithm, simulated annealing, etc. These approaches are effective when it is hard to imagine the optimal structure and difficult to obtain shape derivatives. When one can roughly guess the optimal structure or has only limited design possibilities due to fabrication constraints, one may well be interested in more classical gradient-based optimization methods. This motivated us to investigate shape derivatives of electromagnetic fields produced by complex structures composed of many constituents.

Specifically, we consider the adjoint variable method (AVM) which solves one direct and one adjoint problems to get the full gradients of a certain object function and is therefore considered more efficient than the finite difference which is more costly than AVM when  $p \geq 2$  since it has to solve direct problems at least  $p + 1$  times.

Among numerical solvers widely used for optical problems, such as finite-difference time-domain method, finite element method, we choose the method of moments (MoM) accelerated with the fast multipole method (FMM), which is considered to be attractive in scattering problems. An example of the use of FMM accelerated MoM in metamaterial applications is found in [12] where a conventional (non-periodic) FMM formulation has been utilized. We here use a particular kind of FMM tailored for periodic problems called periodic FMM (pFMM), whose details for Maxwell's equations in 3D are described in [10, 11]. As regards AVM for transmission problems for Maxwell's equations, the fundamentals have been discussed in [13]. As it appears,

however, careful discussions for scattering problems in multidomains with periodic structures are yet to be made.

This paper is organized as follows: Maxwell's equations with periodic boundary conditions and pFMM are discussed in Section 2. The gradients of transmission and reflection coefficients evaluated by AVM are presented in Section 3. Numerical results for verification of AVM and shape optimization of metamaterial are demonstrated in Section 4. The concluding remarks are given at the last section.

## 2. PERIODIC BOUNDARY VALUE PROBLEM

Let  $D$  be a domain in  $\mathbb{R}^3$  defined by

$$D = \left\{ (x_1, x_2, x_3) \mid -\infty < x_1 < \infty, -\frac{L}{2} \leq x_{2,3} \leq \frac{L}{2} \right\},$$

where  $L$  is a positive number called periodic length. The domain  $D$  consists of disjoint periodic subsets  $D_d$ , i.e.,  $D = \bigcup_{d=1}^N \bar{D}_d$ , where  $N$  is the number of subdomains. Among these subdomains, there are two and only two infinite subdomains denoted by  $D_1$  and  $D_N$ , respectively, with  $D_1$  ( $D_N$ ) being the one which extends to  $x_1 \rightarrow -\infty$  ( $+\infty$ ). In  $D_1$ , we consider an incident field denoted by  $(\mathbf{E}^i, \mathbf{H}^i)$ . Also, the set defined by  $S_p = \{\mathbf{x} \mid \mathbf{x} \in \bigcup \partial D_d, |x_2| = L/2 \text{ or } |x_3| = L/2\}$  is called the periodic boundary.

The 2-periodic electromagnetic scattering problem for a periodic structure is defined as follows: One solves Maxwell's equations

$$\begin{aligned} \nabla \times \mathbf{E}(\mathbf{x}) &= i\omega\mu_d\mathbf{H}(\mathbf{x}), & \nabla \times \mathbf{H}(\mathbf{x}) &= -i\omega\varepsilon_d\mathbf{E}(\mathbf{x}), \\ & & \mathbf{x} \in D_d, & \quad d = 1, \dots, N \end{aligned} \quad (2)$$

subject to the boundary condition

$$[[\mathbf{E} \times \mathbf{n}]] = \mathbf{0}, \quad [[\mathbf{H} \times \mathbf{n}]] = \mathbf{0} \quad (3)$$

on the interfaces between subdomains, radiation conditions for the scattered field  $(\mathbf{E}^s, \mathbf{H}^s)$  defined by  $(\mathbf{E} - \mathbf{E}^i, \mathbf{H} - \mathbf{H}^i)$  in  $D_1$ , radiation conditions for  $(\mathbf{E}, \mathbf{H})$  in  $D_N$ , and the periodic boundary condition (PBC) on  $S_p$ . In this statement,  $\mathbf{E}$  and  $\mathbf{H}$  are the electric and magnetic fields,  $\omega$  is the angular frequency,  $\varepsilon_d$  and  $\mu_d$  are the permittivity and permeability of the subdomain  $D_d$ ,  $\mathbf{n}$  is the unit normal vector on the interface with a fixed direction (eventually, we will require  $\mathbf{n}$  on  $\Gamma_{1,N}$  to be outward viewed from  $D_{1,N}$ , respectively, but otherwise the direction of  $\mathbf{n}$  is arbitrary) and  $[[ \ ]]$  is the discontinuity of the enclosed quantity across the interface. Also, we have assumed the  $e^{-i\omega t}$  time dependence

for all relevant quantities where  $i$  stands for  $\sqrt{-1}$ . The PBC for a vector field  $\mathbf{A} = \mathbf{E}, \mathbf{H}$  is written explicitly as

$$\begin{aligned}\mathbf{A}(x_1, L/2, x_3) &= e^{i\beta_2} \mathbf{A}(x_1, -L/2, x_3), \\ \mathbf{A}(x_1, x_2, L/2) &= e^{i\beta_3} \mathbf{A}(x_1, x_2, -L/2)\end{aligned}\quad (4)$$

on  $S_p$ , where  $\beta$  is the phase difference. In the particular case of the incident plane wave, we have  $\beta = (0, k_2^i L, k_3^i L)$  where  $\mathbf{k}^i = (k_1^i, k_2^i, k_3^i)$  is the wave number vector of the incident wave. In the rest of this paper we shall denote the solution to the above problem as

$$(\mathbf{E}, \mathbf{H}) = \mathcal{F}(\mathbf{E}^i, \mathbf{0}, \beta).$$

Similarly, we can consider another problem in which the incident wave  $(\mathbf{E}'^i, \mathbf{H}'^i)$  impinges upon the structure from the  $D_N$  side. The solution to such problem is denoted by

$$(\mathbf{E}, \mathbf{H}) = \mathcal{F}(\mathbf{0}, \mathbf{E}'^i, \beta).$$

Using PMCHWT formulation, we have the electric field integral equation and magnetic field integral equation given bellow [14]:

$$\begin{aligned}\sum_d \int_{\Gamma_d} \mathbf{t}(\mathbf{x}) \cdot \mathbf{E}^i(\mathbf{x}) dS + \sum_d \int_{\Gamma_d} \int_{\Gamma_d} \left\{ \mathbf{t}(\mathbf{x}) \cdot \left[ \mathbf{m}(\mathbf{x}') \times \nabla' G_d^P(\mathbf{x}, \mathbf{x}') \right] \right. \\ \left. - i\omega\mu_d \left[ \mathbf{t}(\mathbf{x}) \cdot \mathbf{j}(\mathbf{x}') - \frac{1}{k_d^2} \nabla_S \cdot \mathbf{t}(\mathbf{x}) \nabla_{S'} \cdot \mathbf{j}(\mathbf{x}') \right] G_d^P(\mathbf{x}, \mathbf{x}') \right\} dS' dS = 0, \quad (5)\end{aligned}$$

$$\begin{aligned}\sum_d \int_{\Gamma_d} \mathbf{t}(\mathbf{x}) \cdot \mathbf{H}^i(\mathbf{x}) dS - \sum_d \int_{\Gamma_d} \int_{\Gamma_d} \left\{ \mathbf{t}(\mathbf{x}) \cdot \left[ \mathbf{j}(\mathbf{x}') \times \nabla' G_d^P(\mathbf{x}, \mathbf{x}') \right] \right. \\ \left. + i\omega\varepsilon_d \left[ \mathbf{t}(\mathbf{x}) \cdot \mathbf{m}(\mathbf{x}') - \frac{1}{k_d^2} \nabla_S \cdot \mathbf{t}(\mathbf{x}) \nabla_{S'} \cdot \mathbf{m}(\mathbf{x}') \right] G_d^P(\mathbf{x}, \mathbf{x}') \right\} dS' dS = 0, \quad (6)\end{aligned}$$

where  $\mathbf{j}(\mathbf{x})$  and  $\mathbf{m}(\mathbf{x})$  are the electric and magnetic currents on the interface defined by

$$\mathbf{j}(\mathbf{x}) = \hat{\mathbf{n}}(\mathbf{x}) \times \mathbf{H}(\mathbf{x}), \quad \mathbf{m}(\mathbf{x}) = \mathbf{E}(\mathbf{x}) \times \hat{\mathbf{n}}(\mathbf{x}), \quad (7)$$

$\hat{\mathbf{n}}$  is the unit normal vector directed outward viewed from  $D_d$ ;  $\mathbf{t}(\mathbf{x})$  is the tangential test function;  $\nabla_S \cdot \mathbf{v} = \nabla \cdot \mathbf{v} - \hat{\mathbf{n}} \cdot \partial \mathbf{v} / \partial \hat{\mathbf{n}}$  denotes the tangential derivative of  $\mathbf{v}(\mathbf{x})$ ;  $k_d = \omega \sqrt{\varepsilon_d \mu_d}$  is the wave number of the subdomain  $D_d$ ;  $\Gamma_d$  is defined by  $\Gamma_d = \partial D_d \setminus S_p$ . We note that  $\Gamma_d$  includes just the interfaces between  $D_d$  and its neighbouring subdomains when  $D_d$  is an infinite one. The periodic Green's function  $G_d^P$  for Helmholtz' equation is given by [10].

$$G_d^P(\mathbf{x}, \mathbf{x}') = \sum_{\omega \in \mathcal{L}} \frac{e^{ik_d |\mathbf{x} - \mathbf{x}' - \omega|}}{4\pi |\mathbf{x} - \mathbf{x}' - \omega|} e^{i\beta \cdot \omega}, \quad (8)$$

where  $\mathcal{L} = \{(0, pL, qL) \mid p, q \in \mathbb{Z}\}$  is the set of lattice points.

These integral equations can be discretized using MoM with the standard RWG basis function and Galerkin testing, and the resulting linear equations can be solved with Krylov subspace iterative methods. The pFMM is used to reduce the cost of matrix-vector product at each iteration using a kernel expansion and a hierarchical recurrence scheme. The pFMM has some differences from traditional FMM. For example, an infinite array of the replica cells are considered in the pFMM so that one can take the periodicity into account. A periodic translation formula is used for the level 0 cell, which includes a lattice sum calculated with the help of Fourier integrals and Poisson's summation formula. We note that metamaterial applications usually consider periodic lengths which are much smaller than the wavelengths. Hence, low frequency FMMs are of interest in many cases. The reader is referred to [10, 11] for further details of pFMM.

### 3. SENSITIVITY ANALYSIS

In studies of metamaterials, one is interested in estimating effective material constants of periodic structures, such as effective refractive index, etc.. Homogenization methods such as Smith's method [6] are utilized to this end. Smith's method uses the following formula to retrieve the effective refractive index  $n$  of a metamaterial from the transmission coefficient  $t$  and the reflection coefficient  $r$  of a layer of periodic structure on a substrate:

$$n = \pm \frac{1}{kd} \arccos \frac{1 + n_g t'^2 - r^2}{[n_g(1+r) + 1-r]t'} + \frac{2\pi m}{kd}, \quad t' = te^{ikdn_g}, \quad (9)$$

where  $d$  is the thickness of the layer,  $k$  the wavenumber of the incident wave in vacuum,  $n_g$  the refractive index of the substrate, and  $m$  an appropriate integer. We use the selection rule of  $m$  given in [7] by checking the continuity of  $\text{Re}(n)$  up to a long wavelength range. The sign of  $\arccos$  can be identified by using the condition  $\text{Im}(n) > 0$ .

The FOM of this metamaterial is then computed with (1). It is of interest to find an optimal structure which maximizes the FOM thus obtained. This motivation leads us to the computation of the reflection and transmission coefficients and their sensitivities with respect to shape parameters of the periodic structure.

#### 3.1. Reciprocity and Reflection and Transmission Coefficients

The well-known reciprocity theorem is useful in the discussion of reflection and transmission coefficients:

**Theorem 1:** Let  $D$  be a bounded domain with a smooth boundary  $\partial D$ . Also, let  $\mathbf{E}_1$  and  $\mathbf{E}_2$  satisfy (the reduced) Maxwell's equations given by

$$\nabla \times (\nabla \times \mathbf{E}_1) = -k^2 \mathbf{E}_1, \quad \nabla \times (\nabla \times \mathbf{E}_2) = -k^2 \mathbf{E}_2, \quad (10)$$

where we have  $k = \omega \sqrt{\mu \varepsilon}$ . Then, we have

$$\int_{\partial D} (\nabla \times \mathbf{E}_1) \cdot (\hat{\mathbf{n}} \times \mathbf{E}_2) dS = \int_{\partial D} (\nabla \times \mathbf{E}_2) \cdot (\hat{\mathbf{n}} \times \mathbf{E}_1) dS. \quad (11)$$

As corollaries to the reciprocity, we have the following well-known results:

**Corollary 1:** Let  $\mathbf{E}_1$  and  $\mathbf{E}_2$  satisfy Maxwell's equations in (10) in a subdomain  $D_d$ . Also, let  $\mathbf{E}_1$  satisfy PBC with  $\beta$  periodicity and let  $\mathbf{E}_2$  satisfy PBC with  $-\beta$  periodicity (i.e., (4) with  $\beta_{2,3}$  replaced by  $-\beta_{2,3}$ ) if  $\partial D_d \cup S_p \neq \emptyset$ . In addition, we require radiation conditions for  $\mathbf{E}_1$  and  $\mathbf{E}_2$  if  $D_d$  is an infinite domain. Then, we have

$$\int_{\Gamma_d} (\nabla \times \mathbf{E}_1) \cdot (\hat{\mathbf{n}} \times \mathbf{E}_2) dS = \int_{\Gamma_d} (\nabla \times \mathbf{E}_2) \cdot (\hat{\mathbf{n}} \times \mathbf{E}_1) dS. \quad (12)$$

This corollary follows immediately from Theorem 1 and (4) if  $D_d$  is a bounded subdomain. If the subdomain under consideration is either of  $D_1$  or  $D_N$  we introduce surfaces  $S_\alpha^\infty$  ( $\alpha = 1$  or  $N$ . We shall use  $\alpha$  exclusively for either 1 or  $N$  in the rest of this paper) as in Figure 1, use Theorem 1 to the bounded domains thus obtained and then let these surfaces tend to infinity to obtain the above corollary.

We now determine the reflection and transmission coefficients with the help of the reciprocity. In general, the electric fields in  $D_\alpha$  ( $\alpha = 1$  or  $N$ ) are written as

$$\mathbf{E} = \sum_{m,n} e^{i\mathbf{k}_{mn}^\alpha \cdot \mathbf{x}} \mathbf{E}_{mn}^\alpha + \mathbf{E}^{i\alpha}, \quad \alpha = 1 \text{ or } N$$

where  $\mathbf{E}^{i\alpha}$  is an incident wave from  $D_\alpha$  ( $\mathbf{E}^{iN}$  is zero for an incidence

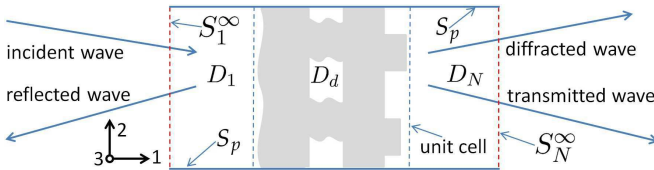


**Figure 1.** The incident, reflected and transmitted waves.

from  $D_1$  and vice versa), and  $\mathbf{k}_{mn}^\alpha$  is a vector defined by

$$\mathbf{k}_{mn}^\alpha = \left( \pm \sqrt{k_\alpha^2 - k_{2m}^2 - k_{3n}^2}, k_{2m}, k_{3n} \right)^T,$$

$$k_{2m} = \frac{2\pi m + \beta_2}{L}, \quad k_{3n} = \frac{2\pi n + \beta_3}{L}, \quad m, n \in \mathbb{Z}$$

and  $\mathbf{E}_{mn}^\alpha$  is a vector perpendicular to  $\mathbf{k}_{mn}^\alpha$ . The double sign in  $\mathbf{k}_{mn}^\alpha$  is positive for  $\alpha = N$  and negative for  $\alpha = 1$ . We can determine the vectors  $\mathbf{E}_{mn}^\alpha$  as follows:

**Corollary 2:** *We have the following results:*

$$\mathbf{F}^\alpha \cdot \mathbf{E}_{mn}^\alpha = \frac{\omega\mu_\alpha}{2L^2\sqrt{k_\alpha^2 - k_{2m}^2 - k_{3n}^2}} \int_{\Gamma_\alpha} \hat{\mathbf{n}} \cdot (\mathbf{m}^{*\alpha} \times \mathbf{j} + \mathbf{j}^{*\alpha} \times \mathbf{m}) dS,$$

where  $\Gamma_\alpha$  is defined by  $\Gamma_\alpha = \partial D_\alpha \setminus (S_p \cup S_\alpha^\infty)$ ,  $\mathbf{j}$  and  $\mathbf{m}$  are defined by (7), and  $\mathbf{j}^{*\alpha} (= \hat{\mathbf{n}} \times \mathbf{H}^{*\alpha})$  and  $\mathbf{m}^{*\alpha} (= \mathbf{E}^{*\alpha} \times \hat{\mathbf{n}})$  are electric and magnetic currents associated with the following inspection fields:

$$\mathbf{E}^{*\alpha} = \mathbf{F}^\alpha e^{-i\mathbf{k}_{mn}^\alpha \cdot \mathbf{x}}, \quad \mathbf{H}^{*\alpha} = -\frac{\mathbf{k}_{mn}^\alpha \times \mathbf{F}^\alpha}{\omega\mu^\alpha} e^{-i\mathbf{k}_{mn}^\alpha \cdot \mathbf{x}},$$

where  $\mathbf{F}^\alpha$  is a unit vector perpendicular to  $\mathbf{k}_{mn}^\alpha$ .

To see this, we argue as in the previous corollary using the electric field produced by  $\mathbf{E}^i$  as  $\mathbf{E}_1$  and the inspection fields  $\mathbf{E}^{*\alpha}$  as  $\mathbf{E}_2$ . Note that the inspection fields  $\mathbf{E}^{*\alpha}$  and  $\mathbf{H}^{*\alpha}$  satisfy the  $-\beta$  periodicity and that contributions from  $S_\alpha^\infty$  are non-zero in the present case.

In metamaterial applications, we may assume that the wavelengths in domains  $D_\alpha$ , denoted by  $\lambda_\alpha$ , satisfy  $\lambda_\alpha > L$ , thus reducing the numbers of both reflected and transmitted plane waves to one. Namely, the vectors  $\mathbf{k}_{mn}^\alpha$  are real only if  $m = n = 0$ . These real vectors are denoted by  $\mathbf{k}^\alpha = \mathbf{k}_{00}^\alpha$  ( $\alpha = 1, N$ ). In this case, we have  $\mathbf{E}_{00}^1 = r\hat{\mathbf{a}}^1$  and  $\mathbf{E}_{00}^N = t\hat{\mathbf{a}}^N$ , respectively, where  $\hat{\mathbf{a}}^\alpha$  are unit vectors. By taking  $\mathbf{F}^\alpha = \hat{\mathbf{a}}^\alpha$ , we have  $r = a_1$  and  $t = a_N$  where

$$a_\alpha = \frac{\omega\mu_\alpha}{2L^2\sqrt{k_\alpha^2 - (k_2^i)^2 - (k_3^i)^2}} \int_{\Gamma_\alpha} \mathbf{n} \cdot (\mathbf{m}^{*\alpha} \times \mathbf{j} + \mathbf{j}^{*\alpha} \times \mathbf{m}) dS.$$

From this formula onward, we assume that the unit normal vector  $\mathbf{n}$  is taken equal to  $\hat{\mathbf{n}}$  on  $\Gamma_\alpha$ .

### 3.2. Sensitivity Analysis for $r$ and $t$

We now compute the sensitivity of  $r$  and  $t$  when the shape of scatterers changes. To this end, we consider any component (denoted by  $\tau$ ) of the shape parameters  $\boldsymbol{\tau}$  introduced in (1). The rate of the shape change is

defined on the boundary of subdomains and is denoted by  $\mathbf{x}_\tau$ . Also, the Eulerian rate of change of field quantities, say  $\mathbf{A}$ , within subdomains is denoted by  $\mathbf{A}_\tau$ .

**Corollary 3:** *The shape sensitivity of the transmission coefficient  $t$  is given as follows:*

$$\begin{aligned} \frac{dt}{d\tau} = & \frac{i\mu_N}{2L^2\sqrt{k_N^2 - (k_2^i)^2 - (k_3^i)^2}} \int_{\Gamma} \left\{ \left[ \frac{1}{\varepsilon} \right] \nabla_S \cdot \mathbf{j} \nabla_S \cdot \boldsymbol{\psi} - \omega^2 \llbracket \mu \rrbracket \mathbf{j} \cdot \boldsymbol{\psi} \right. \\ & \left. - \left( \left[ \frac{1}{\mu} \right] \nabla_S \cdot \mathbf{m} \nabla_S \cdot \boldsymbol{\varphi} - \omega^2 \llbracket \varepsilon \rrbracket \mathbf{m} \cdot \boldsymbol{\varphi} \right) \right\} (\mathbf{x}_\tau \cdot \mathbf{n}) dS, \end{aligned} \quad (13)$$

where  $\Gamma$  is defined by  $\Gamma = \sum_d \Gamma_d$ ;  $\mathbf{j} = \mathbf{n} \times \mathbf{H}$  and  $\mathbf{m} = \mathbf{E} \times \mathbf{n}$  are the electric and magnetic currents associated with  $(\mathbf{E}, \mathbf{H}) = \mathcal{F}(\mathbf{E}^i, \mathbf{0}, \boldsymbol{\beta})$  with  $\mathbf{E}^i = \widehat{\mathbf{E}}^i e^{i\mathbf{k}^i \cdot \mathbf{x}}$ ;  $\boldsymbol{\psi} = \mathbf{n} \times \mathbf{G}$  and  $\boldsymbol{\varphi} = \mathbf{F} \times \mathbf{n}$  are the electric and magnetic currents associated with the electromagnetic field  $(\mathbf{F}, \mathbf{G}) = \mathcal{F}(\mathbf{0}, \mathbf{E}^{*i}, -\boldsymbol{\beta})$  with  $\mathbf{E}^{*i} = \widehat{\mathbf{a}}^N e^{-i\mathbf{k}^N \cdot \mathbf{x}}$ . Also,  $\llbracket f \rrbracket$  is defined by  $\llbracket f \rrbracket = f^- - f^+$  where  $f^+$  indicates the limit on  $\Gamma$  from the side into which  $\mathbf{n}$  points and  $f^-$  the opposite limit.

*Proof.* The reader is referred to Appendix A for a proof.

Similarly, the sensitivity of the reflection coefficient  $r$  can be evaluated by

$$\begin{aligned} \frac{dr}{d\tau} = & \frac{i\mu_1}{2L^2\sqrt{k_1^2 - (k_2^i)^2 - (k_3^i)^2}} \int_{\Gamma} \left\{ \left[ \frac{1}{\varepsilon} \right] \nabla_S \cdot \mathbf{j} \nabla_S \cdot \boldsymbol{\psi}' - \omega^2 \llbracket \mu \rrbracket \mathbf{j} \cdot \boldsymbol{\psi}' \right. \\ & \left. - \left( \left[ \frac{1}{\mu} \right] \nabla_S \cdot \mathbf{m} \nabla_S \cdot \boldsymbol{\varphi}' - \omega^2 \llbracket \varepsilon \rrbracket \mathbf{m} \cdot \boldsymbol{\varphi}' \right) \right\} (\mathbf{x}_\tau \cdot \mathbf{n}) dS, \end{aligned} \quad (14)$$

where  $\boldsymbol{\psi}'$  and  $\boldsymbol{\varphi}'$  are the electric and magnetic currents associated with the electromagnetic field  $(\mathbf{F}', \mathbf{G}') = \mathcal{F}(\mathbf{E}^{*i}, \mathbf{0}, -\boldsymbol{\beta})$  with  $\mathbf{E}^{*i} = \widehat{\mathbf{a}}^1 e^{-i\mathbf{k}^1 \cdot \mathbf{x}}$ .

Specifically, when the scatterer is symmetric with respect to  $x_3$  axis and the incident wave  $\mathbf{E}^i$  is polarized in  $x_2$  direction and is of normal incidence, we have  $\mathbf{k}^i = (k_1, 0, 0)^T = -\mathbf{k}^1$ ,  $\widehat{\mathbf{a}}^1 = \widehat{\mathbf{E}}^i = \mathbf{e}_2$  and, hence,  $\boldsymbol{\psi}' = \mathbf{j}$  and  $\boldsymbol{\varphi}' = \mathbf{m}$ .

#### 4. NUMERICAL RESULTS

In this section, we validate our formulation for AVM via a simple test problem where an analytical solution is available. We then apply our method to an optimal design of an optical metamaterial having a DF

structure, in which we maximize the FOM while keeping the effective refractive index negative. For the calculation, we use FUJITSU HX600 supercomputer of Academic Center for Computing and Media Studies of Kyoto University. The CPU of this computer is AMD Quad Core Opteron, 2.3 GHz. The code is OpenMP parallelized and linear equations in pFMM are solved with FGMRES [15] with the relative error of  $10^{-3}$  used as the criterion of convergence. A free software GMSH is used to generate the surface mesh.

### 4.1. Validation of AVM

In order to check the accuracy of our AVM computation, we use a dielectric slab on a glass substrate as a model for validation, i.e., we consider a layer of dielectric material between vacuum and an infinite glass substrate. The refractive index of slab and substrate are 1.65 and 1.51 respectively. The incident wave is a plane electromagnetic wave of the normal incidence from the vacuum side; the wavelength in vacuum is  $\lambda = 824$  nm; the thickness of slab is  $\tau$ ; the periodic length is  $L = 600$  nm. The interface is discretized into uniform isosceles right triangle meshes with side lengths of  $L/30$ . The gradient  $dt/d\tau$  evaluated with AVM and that obtained with analytical solution of  $t(\tau)$  are compared in Figure 2, where the origin is defined at the incident surface. From this figure, we can see that the gradients calculated by AVM have a good agreement with analytical results.

### 4.2. Shape Optimization of Metamaterials

We now proceed to the shape optimization problem. We consider a DF structure shown in Figure 3, which includes the top view (inset) and the detail and mesh for the unit cell. This structure consists of two silver layers having the thickness of  $\tau_1$  separated by a dielectric layer having the thickness of  $\tau_2$ . The structure is perforated periodically with a

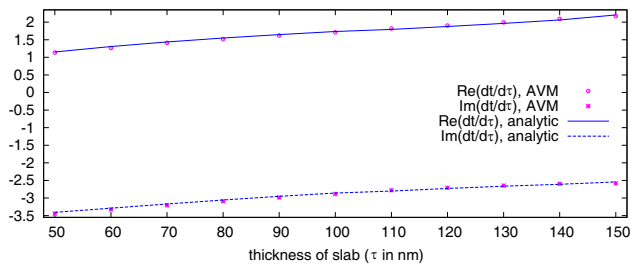
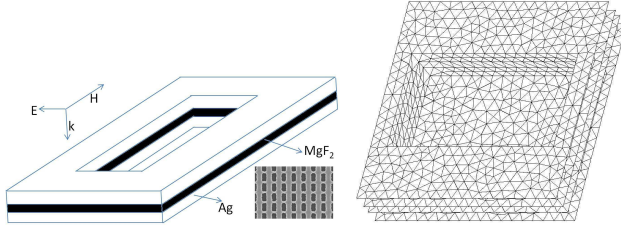


Figure 2. AVM and analytical results of  $dt/d\tau$  for dielectric slab.



**Figure 3.** A periodic cell of DF-grating and its interface mesh.

periodic length of  $L = 300$  nm in both  $x_2$  and  $x_3$  directions. The holes are rectangular and parallel to  $x_2$  and  $x_3$  axes. The line widths of the silver film in  $x_2$  and  $x_3$  directions are denoted by  $\tau_3$  and  $\tau_4$ , where  $x_1$ ,  $x_2$  and  $x_3$  axes are in the directions of  $\mathbf{k}$ ,  $\mathbf{E}$  and  $\mathbf{H}$  shown in Figure 3. This structure is on a semi-infinite glass substrate, and the rest of the space is void. We consider an incident plane wave of normal incidence from the vacuum side, whose electric field is polarized in  $x_2$  direction and whose wavelength in vacuum is  $\lambda = 780$  nm. This structure is close (but not identical) to the one considered by Dolling et al. [3]. For the purpose of comparison, we use the same material parameters as have been used by Dolling et al. Namely, the refractive indices of glass substrate and  $\text{MgF}_2$  dielectric layer are 1.5 and 1.38, and the plasma and collision frequencies for silver are  $\omega_p = 1.37 \times 10^{16}$  (1/s) and  $\omega_c = 9.0 \times 10^{13}$  (1/s) in the Drude model, respectively. We follow Dolling et al. to take  $\omega_c$  much larger than the bulk metal value found in [16], considering the surface roughness.

In the optimization, the object function is defined as

$$\min_{\boldsymbol{\tau}} J = -\text{FOM} + 10^4 \max\{\text{Re}(n) + 0.1, 0\}. \quad (15)$$

The 2nd term is the penalty which keeps  $\text{Re}(n) \leq -0.1$ . The initial guesses for  $\tau_i$  ( $i = 1, \dots, 4$ ) are chosen such that this condition for  $\text{Re}(n)$  is satisfied. Also, the shape parameters are constrained in  $\tau_i \in (L_1^i, L_2^i)$  using new parameters  $\sigma_i$  defined by

$$\tau_i = \frac{L_2^i - L_1^i}{\pi} \tan^{-1} \sigma_i + \frac{L_2^i + L_1^i}{2}.$$

Design variables are updated iteratively by the limited memory version of BFGS method (LM-BFGS) [17] with the Armijo condition for the linear search. This process requires the evaluation of the gradient  $dJ/d\boldsymbol{\tau}$ , which can be obtained from (13) and (14) and the evaluation of  $\mathbf{x}_{\boldsymbol{\tau}} \cdot \mathbf{n}$  in these formulas is easy. When the shape parameters are updated at each linear search and LM-BFGS iteration step, a new

surface mesh can be generated automatically by GMSH. A sample mesh for the unit cell of the DF grating structure is given in Figure 3.

#### 4.2.1. Verification

We first test the AVM calculation of  $dJ/d\tau$ . Assume that the thicknesses of silver and dielectric layers are  $\tau_1 = 52$  nm and  $\tau_2 = 15$  nm, and the line widths of silver films at  $x_2$  and  $x_3$  directions are  $\tau_3 = 126$  nm and  $\tau_4 = 58$  nm, respectively. We choose 4 different meshes ( $lc/L = 0.02, 0.015, 0.01$  and  $0.0075$ ) to compare the accuracy of AVM and finite difference, where  $lc$  is a mesh parameter roughly equal to the average edge length of patches. Central difference  $(f(\tau+\epsilon/2)-f(\tau-\epsilon/2))/\epsilon$  is used in finite difference with  $\epsilon = 10^{-4}L$ . Derivatives calculated by AVM and finite difference for DF grating are listed in Table 1. As we can see from Table 1, the gradients calculated by finite difference and AVM have some difference, but they converge to the same values as one refines the mesh. As a matter of fact, Table 1 shows that the convergence of AVM results is faster than that of finite difference as one refines the mesh. Therefore, one may expect that the gradient evaluated by AVM is more accurate than the finite difference results obtained with the same mesh, and that AVM can meet a practical accuracy requirement with a coarser mesh than finite difference. Indeed, the AVM results with  $lc = 0.015L$  is accurate to within 6% of those with  $lc = 0.0075L$ . A similar conclusion has been reached by Veronis et al. [18] for a sensitivity analysis of nanophotonic devices using AVM.

**Table 1.** AVM and finite difference (FD) results with different meshes.

	$lc/L$	$dJ/d\tau_1$	$dJ/d\tau_2$	$dJ/d\tau_3$	$dJ/d\tau_4$
AVM	0.02	4.18	-29.76	-0.59	7.37
	0.015	4.24	-29.90	-0.69	7.10
	0.01	4.17	-30.04	-0.66	7.15
	0.0075	4.15	-30.09	-0.65	7.17
FD	0.02	4.32	-30.69	-0.95	6.75
	0.015	3.78	-30.53	-0.87	6.82
	0.01	4.10	-30.20	-0.63	6.97
	0.0075	4.13	-30.11	-0.65	7.13

#### 4.2.2. Shape Optimization

We now apply the methods developed so far to the optimization problem. We carry out this optimization in three stages in order to reduce the run time. Namely, we start from the initial guess using a coarse mesh with  $lc = 0.05L$ . In the second stage, we repeat the process in the first stage using the final result of the first stage as the initial guess and a medium mesh obtained with  $lc = 0.02L$ . The result of the second stage gives a fairly good initial guess, with which we switch to a fine mesh ( $lc = 0.015L$ ) so that we can maximize FOM with higher accuracy. The convergence criterion for the LM-BFGS optimization method is  $\|\mathbf{g}_k\|_2 \leq 10^{-3}$  in the third stage, while we terminate first and second stages when the object function ceases to increase.

The FOM obtained at each iteration step is shown in Figure 4, and the shape parameters at the initial, (two) switching and final steps are given in Table 2. The refractive index and FOM of the DF grating with the optimal shape parameters in Table 2 at different wavelengths are shown in Figure 5.

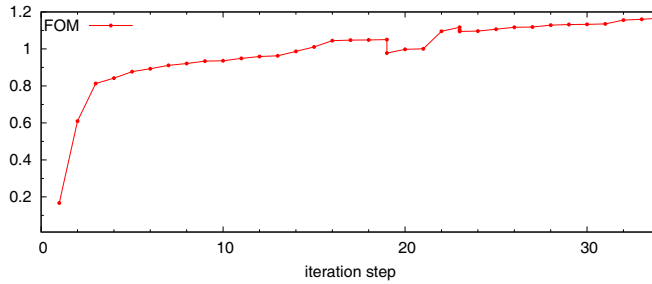


**Figure 4.** Convergence of FOM with LM-BFGS.

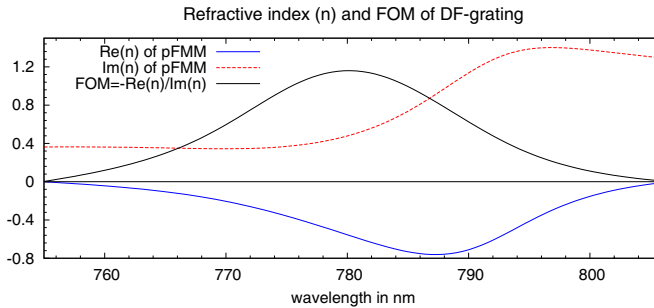


**Figure 5.** The refractive index and FOM of DF-grating.

**Table 2.** Shape parameters at initial, switching and final steps, in nm.

step	$\tau_1$	$\tau_2$	$\tau_3$	$\tau_4$
1	52	15	126	58
19	63.802	15.022	117.582	55.405
23	66.315	15.035	117.804	52.510
34	65.473	15.159	118.333	51.732

From Figure 4, we can see that FOM increases steadily when shape parameters are updated. At steps 19 and 23, we observe switching error since we change meshes. At the final step the maximum FOM reaches 1.166 at 780 nm, where  $n = -0.553 + 0.474i$ . In Figure 5, we can see that the NIM spectral range is 755–806 nm, and the maximum FOM is reached also at 780 nm, where FOM is maximized.

Typical run time and the number of FGMRES iterations for one solution of boundary integral equations are about 3 minutes and 105 with the coarse mesh with  $lc = 0.05L$  (4587 edges) and about 47 minutes and 193 with the fine mesh with  $lc = 0.015L$  (55857 edges). The total run time for the whole optimization is about 2.7 days and the amount of memory use is about 8 GB.

In [3], Dolling et al. could realize an FOM of 0.5 at 780 nm with a slightly distorted rectangular hole. Compared with their result, our final FOM is more than 2 times larger, so the shape optimization method seems to be feasible and effective in improving FOM. This result clearly shows that small changes of the thickness of each layer and the shape size of the rectangular hole have a large influence on the loss of metamaterial. However, the implication of this result in real DF structures may need careful assessment since the fabrication of nanoscale structures still has limited precision.

## 5. CONCLUDING REMARKS

- In this paper, we have discussed shape derivatives of electromagnetic fields produced by 2-periodic structures. The shape derivatives of the farfields are calculated with AVM, and the forward and adjoint problems of AVM are solved with pFMM. AVM is more efficient than finite difference since AVM solves Maxwell's equations twice no matter how many shape parameters one may have. AVM is found useful for the shape design of negative-index metamaterial with multi-parameters.
- In PMCHWT formulation it is very important to use good

preconditioners. The present investigation followed [10] to use the nearfield contribution of the system matrix computed explicitly in FMM as the preconditioner. Unfortunately, however, this preconditioner is not efficient enough in the metamaterial applications to carry out the whole optimization with the fine mesh only. The use of other preconditioners such as those based on Calderon's formulas [19] will be a future research subject.

- A preliminary test shows that the use of the steepest descent method in the first stage of the optimization may further decrease the run time. An investigation along this line is under way.

## ACKNOWLEDGMENT

This work is funded partly by Grand in Aid for Scientific Researches of Ministry of Education, Culture, Sports, Science and Technology, Japan. The authors would like to express their gratitude to Mr. Y. Kurami of Nomura Research Institute since this work is based on his work carried out in Kyoto University while he was a graduate student. Acknowledgement is also due to Prof. T. Ishihara of Tohoku University for his guidance and discussions.

## APPENDIX A. A PROOF OF COROLLARY 3

This Appendix presents a proof of Corollary 3.

We first note that  $(\mathbf{E}_\tau, \mathbf{H}_\tau)$  satisfies Maxwell's equations and that  $dt/d\tau$  and  $dr/d\tau$  are the magnitudes of  $\mathbf{E}_\tau$  in the far field. We can therefore apply Corollary 2 to  $(\mathbf{E}_\tau, \mathbf{H}_\tau)$  to obtain

$$\frac{dt}{d\tau} = \frac{\omega\mu_N}{2L^2\sqrt{k_N^2 - (k_2^i)^2 - (k_3^i)^2}} \int_{\Gamma_N} \mathbf{n} \cdot (\mathbf{m}^{*N} \times \mathbf{j}_\tau + \mathbf{j}^{*N} \times \mathbf{m}_\tau) dS,$$

where  $\mathbf{m}^{*N}$  and  $\mathbf{j}^{*N}$  are defined in Corollary 2. This is followed by a repeated use of Corollary 1, which yields

$$\frac{dt}{d\tau} = \frac{\omega\mu_N}{2L^2\sqrt{k_N^2 - (k_2^i)^2 - (k_3^i)^2}} \int_{\Gamma} \mathbf{n} \cdot (\boldsymbol{\varphi} \times \llbracket \mathbf{j}_\tau \rrbracket + \boldsymbol{\psi} \times \llbracket \mathbf{m}_\tau \rrbracket) dS,$$

where

$$\llbracket \mathbf{j}_\tau \rrbracket = \llbracket \mathbf{n} \times \mathbf{H}_\tau \rrbracket, \quad \llbracket \mathbf{m}_\tau \rrbracket = \llbracket \mathbf{E}_\tau \times \mathbf{n} \rrbracket.$$

On the other hand, we use (3) to obtain

$$\begin{aligned} \llbracket \mathbf{m}_\tau \rrbracket &= i\omega\llbracket \mu \rrbracket (\mathbf{j} \times \mathbf{n})(\mathbf{x}_\tau \cdot \mathbf{n}) - (\nabla_S \times \llbracket \mathbf{E} \rrbracket)(\mathbf{x}_\tau \cdot \mathbf{n}), \\ \llbracket \mathbf{j}_\tau \rrbracket &= -i\omega\llbracket \varepsilon \rrbracket (\mathbf{m} \times \mathbf{n})(\mathbf{x}_\tau \cdot \mathbf{n}) + (\nabla_S \times \llbracket \mathbf{H} \rrbracket)(\mathbf{x}_\tau \cdot \mathbf{n}). \end{aligned}$$

In these formulae, the tangential derivatives apply to all the terms to the right of them. Substitution of these results in (13), followed by the use of integration by parts, gives the desired results.

## REFERENCES

1. Pendry, J. B., "Negative refraction makes a perfect lens," *Phys. Rev. Lett.* Vol. 85, 3966–3969, 2000.
2. Zhang, S., W. Fan, N. Panoiu, R. Osgood, and S. Brueck, "Experimental demonstration of near-infrared negative-index metamaterials," *Phys. Rev. Lett.*, Vol. 95, No. 13, 137404, 2005.
3. Dolling, G., M. Wegener, C. M. Soukoulis, and S. Linden, "Negative-index metamaterial at 780 nm wavelength," *Opt. Lett.*, Vol. 32, No. 1, 53–55, 2007.
4. Valentine, J., S. Zhang, T. Zentgraf, and X. Zhang, "Development of bulk optical negative index fishnet metamaterials: Achieving a low-loss and broadband response through coupling," *Proceedings of the IEEE*, Vol. 99, No. 10, 1682–1690, 2011.
5. Dolling, G., C. Enkrich, C. Soukoulis, and S. Linden, "Design-related losses of double-fishnet negative-index photonic metamaterials," *Opt. Express*, Vol. 15, No. 18, 11536–11541, 2007.
6. Smith, D. R. and S. Schultz, "Determination of effective permittivity and permeability of metamaterials from reflection and transmission coefficients," *Phys. Rev.*, Vol. B65, 195104, 2002.
7. Kildishev, A. V., U. K. Chettiar, Z. Liu, V. M. Shalaev, D.-H. Kwon, Z. Bayraktar, and D. A. Werner, "Stochastic optimization of low-loss optical negative-index metamaterial," *J. Opt. Soc. Am. B*, Vol. 24, A34–A39, 2007.
8. Bossard, J. A., S. Yun, D. H. Werner, and T. S. Mayer, "Synthesizing low loss negative index metamaterial stacks for the mid-infrared using genetic algorithm," *Opt. Express*, Vol. 17, 14771–14779, 2009.
9. Zhao, Y., F. Chen, Q. Shen, Q. Liu, and L. Zhang, "Optimizing low loss negative index metamaterial for visible spectrum using differential evolution," *Opt. Express*, Vol. 19, 11605–11614, 2011.
10. Otani, Y. and N. Nishimura, "A periodic FMM for Maxwell's equations in 3D and its applications to problems to photonic crystals," *J. Comput. Phys.*, Vol. 227, No. 9, 4630–4652, 2008.
11. Otani, Y. and N. Nishimura, "An FMM for orthotropic periodic boundary value problems for Maxwell's equations," *Waves in Random and Complex Media*, Vol. 19, No. 1, 80–104, 2009.

12. Ergül, Ö. and L. Gürel, "Efficient solutions of metamaterial problems using a low-frequency multilevel fast multipole algorithm," *Progress In Electromagnetics Research*, Vol. 108, 81–99, 2010.
13. Bondeson, A., Y. Yang, and P. Weinerfelt, "Shape optimization for radar cross sections by a gradient method," *Int. J. Num. Meth. Eng.*, Vol. 61, 687–715, 2004.
14. Chew, W. C., J. M. Jin, E. Michielssen, and J. M. Song, *Fast and Efficient Algorithms in Computational Electromagnetics*, Artech House, Boston, 2001.
15. Frayssé, V., L. Giraud, S. Gratton, and J. Langou, "Algorithm 842: A set of GMRES routines for real and complex arithmetics on high performance computers," *ACM Trans. Math. Softw.*, Vol. 31, No. 2, 228–238, 2005.
16. Johnson, P. B. and R. W. Christy, "Optical constants of the noble metals," *Phys. Rev. B*, Vol. 6, 4370–4379, 1972.
17. Byrd, R. H., J. Nocedal, and R. B. Schnabel, "Representations of quasi-Newton matrices and their use in limited memory methods," *Mathematical Programming*, Vol. 63, No. 4, 129–156, 1994.
18. Veronis, G., R. W. Dutton, and S. Fan, "Method for sensitivity analysis of photonic crystal devices," *Opt. Lett.*, Vol. 29, No. 19, 2288–2290, 2004.
19. Niino, K. and N. Nishimura, "Preconditioning based on Calderon's formulae for periodic fast multipole methods for Helmholtz' equation," *J. Comput. Phys.*, Vol. 231, 66–81, 2012.